Stability of the flow due to a linear stretching sheet

Griffiths, P., Stephen, S. & Khan, M.

Stability of the flow due to a linear stretching sheet

P. T. Griffiths,[1] S. O. Stephen,[2] and M. Khan[3]

[1]*Centre for Fluid and Complex Systems, Coventry University, Coventry CV1 5FB, United Kingdom*

[2]*School of Mathematics and Statistics, The University of Sydney, Sydney NSW 2006, Australia*

[3]*Department of Mathematics, Quaid-i-Azam University, Islamabad 45320, Pakistan*

(*Electronic mail: paul.griffiths@coventry.ac.uk)

In this article we consider the linear stability of the two-dimensional flow induced by the linear stretching of a surface in the streamwise direction. The basic flow is a rare example of an exact analytical solution of the Navier-Stokes equations. Using results from a large Reynolds number asymptotic study and a highly accurate spectral numerical method we show that this flow is linearly unstable to disturbances in the form of Tollmien-Schlichting waves. Previous studies have shown this flow is linearly stable. However, our results show that this is only true for Görtler-type disturbances.

I. INTRODUCTION

Boundary-layer flows induced by the extrusion of a surface have received considerable attention since they were first described by Sakiadis[1]. Interest in these types of flows stems not only from the fact that they often admit analytical solutions to the Navier-Stokes equations; they are also used to model a variety of industrial processes. These so called 'stretching' flows are of practical importance to chemical and metallurgy industries where extrusion processes are commonplace. One such example would be the manufacture of a polymer sheet being continuously extruded from a casting die. Bounded stretching and/or shrinking surface flows also have a number of physiological applications and can be used to model transmyocardial laser revascularisation (TMLR), see, for example Waters[2].

These types of boundary-layer flows exhibit fluid entrainment and are therefore qualitatively different to Blasius-type boundary layer flows. In fact, two- and three-dimensional stretching flows are much more closely aligned to stagnation-point flows. The specific focus of this article will be on flows induced by an impermeable sheet with a velocity that increases linearly in the direction of stretching. Vleggaar[3] has shown that this linear behaviour is appropriate in relevant experiments. This specific case of linear stretching was first considered by Crane[4] who derived an exact analytical solution of the Navier-Stokes equations in two dimensions. The equivalent three-dimensional problem was first considered by Wang[5] who demonstrated that although exact analytical solutions could not be obtained, the problem could be solved numerically by introducing a suitable similarity approach. Given that these flows exhibit fluid entrainment at the boundary-layer edge, and that the surface stretching is linear in nature, an association can be made between these flows and the three-dimensional flow induced by a rotating disk. Very recently the ideas of Crane and Wang have been extended by Ayats *et al.*[6] to include the family of flows associated with the independent stretching or shrinking of two infinite parallel plates.

A wealth of literature exists concerning flows over different types of stretching surfaces. Crane's analysis of the flow induced by a linear sheet velocity has been extended to consider power-law type sheet velocities by Vleggaar[3], and exponential type sheet velocities by Magyari and Keller[7]. Gupta and Gupta[8], included the effects of both permeability and heat and mass transfer demonstrating that exact analytical solutions for the temperature variation across the layer can be obtained in the case when the Prandtl number is equal to unity. In the cases when this condition does not hold the solutions can be generalised and are described in terms of the in-

complete gamma function. The relatively recent article by Al-Housseiny and Stone[9] provides a chronological summary of the literature on boundary-layer flows due to stretching impermeable sheets and the interested reader is referred to this manuscript for a more comprehensive list of previous studies. In addition to the studies noted by Al-Housseiny and Stone[9], there are many more studies that consider these types of flows with the addition of magnetohydrodynamic (Chakrabarti and Gupta[10]), non-Newtonian (Rajagopal, Na, and Gupta[11]) and pressure gradient (Riley and Weidman[12]) effects. There are yet more studies that consider combinations of these effects for permeable/impermeable stretching (or indeed shrinking) sheets, one particularly nice example is Liao's investigation[13], which details a range of analytical solutions for magnetohydrodynamic non-Newtonian stretching flows.

Given the vast number of studies detailing basic flow solutions for a plethora of different stretching configurations, it is surprising just how little attention the associated stability problems have received. Bhattacharyya and Gupta[14], were the first to investigate the linear stability of the two-dimensional Crane solution, determining that the flow is linearly stable to infinitesimal Görtler-type disturbances. Seeking disturbances of this nature is an entirely justifiable procedure since the flow exhibits streamline curvature. It is well understood that Görtler-type disturbances form owing to centrifugal instability. This is in contrast to Tollmien-Schlichting (TS) waves that are observed in flows that exhibit zero curvature at the wall, such as the Blasius boundary-layer, and the stretching sheet configuration consider herein. Indeed, Bhattacharyya and Gupta[14] note that "...*our stability analysis is confined to infinitesimal Görtler-type disturbances, which are non-propagating. It cannot, therefore, be ruled out that the flow may be unstable to other types of disturbances which may be infinitesimal or of finite amplitude*". Bhattacharyya and Gupta's analysis was then extended by Takhar, Ali, and Gupta[15] to include magnetohydrodynamic effects. The authors note that the magnetic field has a stabilising influence on a flow that was already linearly stable. In much the same fashion, Dandapat, Holmedal, and Andersson[16] consider an extension to include viscoelastic fluid effects, determining that, for disturbance wavelengths shorter than the viscoelastic lengthscale, the flow will again be further stabilised.

More recently Davis and Pozrikidis[17] have revisited the linear stability of the flow induced by a linear stretching sheet. In a departure from the analysis of Bhattacharyya and Gupta[14], the authors stipulate that the streamwise dependence of the disturbances must match that of the base state. Again, searching for Görtler-type disturbances, they find that the flow is linearly stable to both two- and three-dimensional disturbances. A far-field asymptotic analysis details a remarkably

simple relationship between the growth rate of the disturbance and the disturbance wavenumber. The work associated in the derivation of this relationship offers an insight as to why this flow is not susceptible to this type of disturbance.

In this study we will analyse the stability of Crane's solution from an alternative viewpoint. Rather than seeking disturbances of Görtler-type we will instead investigate the possibility of the development of small-amplitude perturbations in the form of TS waves. TS instability waves are a prominent feature of many flat plate boundary-layer flows and their growth has been shown to be well described by linear stability theory. It is clear from the statements of Bhattacharyya and Gupta that the importance of these types of disturbances in stretching flows has been known about for some time. Within this investigation we will outline both asymptotic and numerical stability analyses that show that Crane's flow is, in fact, linearly *unstable* to small-amplitude TS waves.

In II A we formulate the problem and derive the governing perturbation equations. In II B we describe our numerical scheme in detail and validate it against the results of Davis and Pozrikidis[17]. In II C we derive the appropriate energy balance equations for problems of this type. Having completed these derivations and our validation exercise, in III, we present linear stability results for two- and three-dimensional disturbances and also results from our integral energy analysis, which provides insights as to the mechanisms responsible for this observed instability. In IV our numerical results are compared to high Reynolds number asymptotic predictions, where we focus primarily on the most unstable case, 2D perturbations. Excellent agreement is observed between our asymptotic and numerical findings. Lastly, in V, our results are discussed and placed in context and potential avenues for further work are outlined.

II. PROBLEM FORMULATION AND VALIDATION OF THE NUMERICAL SCHEME

A. Derivation of the basic state and the governing perturbation equations

We consider the flow of a steady, incompressible, Newtonian fluid induced by the stretching of an infinite planar surface. The streamwise, wall-normal and spanwise coordinates are x^*, y^*, and z^*, respectively. The associated fluid velocities in these directions are then $\tilde{\mathbf{U}}^* = (\tilde{U}^*, \tilde{V}^*, \tilde{W}^*)$. The surface stretching acts along the $y^* = 0$ plane and is linear in nature. Note that throughout this analysis an asterisk indicates a dimensional quantity.

The system is governed by the following conservation of mass and momentum equations

$$\nabla^* \cdot \tilde{\mathbf{U}}^* = 0, \tag{1a}$$

$$\frac{D\tilde{\mathbf{U}}^*}{Dt^*} = -\frac{1}{\rho^*}\nabla^*\tilde{P}^* + v^*\Delta^*\tilde{\mathbf{U}}^*, \tag{1b}$$

where t^* is time, ρ^* is the fluid density, $\tilde{P}^*$ is pressure and v^* is the kinematic viscosity of the fluid. The two-dimensional mean flow (see Fig. 1 (a)) is solved subject to the following boundary conditions

$$\tilde{U}^*(y^* = 0) - \xi^* x^* = \tilde{V}^*(y^* = 0) = 0, \quad \tilde{U}^*(y^* \to \infty) \to 0, \tag{2}$$

where the constant ξ^* is the stretching rate with units s^{-1}. The exact solution of (1) subject to (2) was first reported by Crane[4]. By introducing the following similarity variables

$$U(y) = \frac{\tilde{U}^*}{\xi^* x^*}, \quad V(y) = \frac{\tilde{V}^*}{\sqrt{\xi^* v^*}}, \quad P(y) = \frac{\tilde{P}^*}{\rho^* \xi^* x^*},$$

where $y = y^*/L^*$, and the non-dimensionalising length-scale is $L^* = \sqrt{v^*/\xi^*}$, the governing equations are reduced to the following set of coupled non-linear ODEs

$$U + V' = 0,$$

$$U^2 + VU' = U'',$$

$$VV' = -P' + V''.$$

These must be solved subject to

$$U(y = 0) - 1 = V(y = 0) = 0, \quad U(y \to \infty) \to 0.$$

As noted by Crane[4], the streamwise and wall-normal velocities and pressure have a remarkably simple analytical solution

$$U = e^{-y}, \quad V = e^{-y} - 1, \quad P = P_0 + \frac{(1 - e^{-2y})}{2},$$
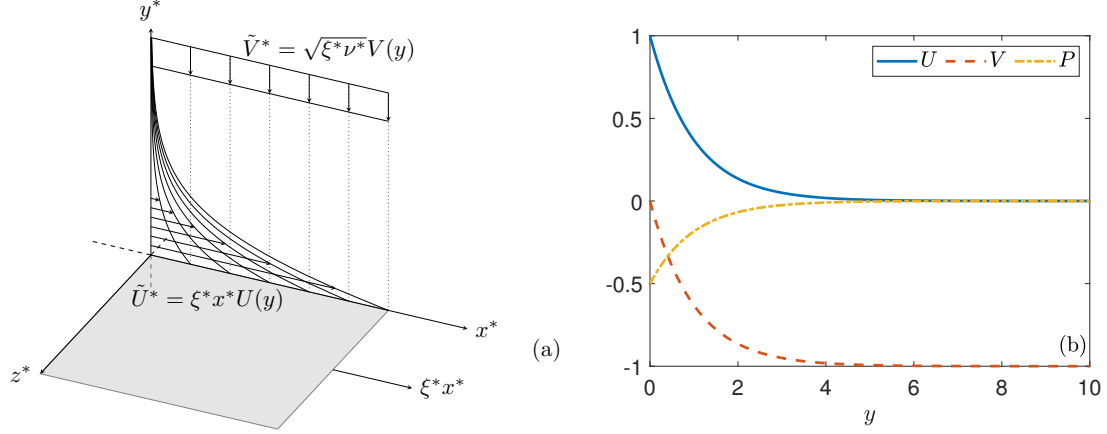
FIG. 1. Basic flow profiles induced by a linear stretching sheet. A schematic diagram of the flow is presented in (a). The streamwise profile $\tilde{U}^* = \xi^* x^* U(y)$, linearly increases with the streamwise coordinate. The wall-normal flow component is independent of the streamwise coordinate and, far away from the wall, is directed towards the stretching surface with uniform velocity $\tilde{V}_\infty^* = -\sqrt{\xi^* \nu^*}$. The exact similarity profiles are presented in (b). To ensure that the reference pressure at the edge of the boundary layer is zero, the constant P_0 is set equal to minus one-half.

where $P_0 = P(y = 0)$. These solutions are highlighted in Fig. 1 (b). The stability analysis is then applied at a streamwise location x_s^*. The local Reynolds number is $R = x_s^* \xi^* L^* / \nu^* = x_s^* / L^* = x_s$. Thus, the local Reynolds number is identically equivalent to a dimensionless streamwise location along the stretching sheet. In this sense, this flow is representative of the two-dimensional equivalent of the flow due to a rotating disk where one finds that a radial location along the disk is equivalent to the local Reynolds number[18]. The non-dimensionalising velocity, pressure and time-scales are then $x_s^* \xi^*$, $\rho^* (x_s^* \xi^*)^2$ and $L^* / (x_s^* \xi^*)$.

After non-dimensionalisation the mean flow quantities are perturbed as follows

$$\tilde{U}(x,y,z,t) = \frac{x}{R} U(y) + u(x,y,z,t),$$
$$\tilde{V}(x,y,z,t) = \frac{1}{R} V(y) + v(x,y,z,t),$$
$$\tilde{W}(x,y,z,t) = \qquad\quad + w(x,y,z,t),$$
$$\tilde{P}(x,y,z,t) = \frac{1}{R^2} P(y) + p(x,y,z,t),$$

where the perturbation quantities (u, v, w, p) are assumed to be small. The dimensionless governing equations are then linearised with respect to the perturbation quantities. In order to make the

6

perturbation equations separable in x, y and t, it is necessary to invoke a parallel-flow-type approximation; that is to say that the variable x is replaced throughout by the Reynolds number R. This is consistent with the approach adopted by Lingwood[18], in her corresponding three-dimensional rotating disk analysis, where the spatial variable r is replaced by R. Although the flow is not strictly homogeneous in the streamwise direction it is reasonable to make this parallel-flow-type approximation given that we expect the onset of linear instability to occur sufficiently far enough downstream (i.e., at reasonably large Reynolds numbers) from the leading edge. Employing this approximation leads to the retention of the terms associated with the wall-normal mean velocity profile V. This is a departure from Blasius-type flat plate boundary-layer studies but is consistent with Lingwood's approach where she also retains terms associated with the wall-normal velocity profile (in her case this is W, not V, since the flow over a rotating disk is three-dimensional, not two-dimensional). The resulting system of linear perturbation equations is then

$$\nabla \cdot \boldsymbol{u} = 0, \tag{3a}$$

$$\mathscr{L}\boldsymbol{u} + \left(U'v + \frac{Uu}{R}\right)\hat{\boldsymbol{x}} + \frac{V'v}{R}\hat{\boldsymbol{y}} = -\nabla p + \frac{1}{R}\Delta\boldsymbol{u}, \tag{3b}$$

where $\boldsymbol{u} = (u, v, w)$, the operator $\mathscr{L}$ is defined like so

$$\mathscr{L} = \frac{\partial}{\partial t} + U\frac{\partial}{\partial x} + \frac{V}{R}\frac{\partial}{\partial y},$$

and $\hat{\boldsymbol{x}}$ and $\hat{\boldsymbol{y}}$ are the unit vectors in the streamwise and wall-normal directions, respectively. At this stage it is worth noting that the last two terms on the left-hand side of (3b), and the final term associated with the operator $\mathscr{L}$, appear due to the x-dependence of the streamwise velocity component and the non-zero nature of the wall-normal velocity component. The retention of these terms is entirely consistent with the three-dimensional analysis presented by[18] and ensures that the action of surface stretching is considered explicitly. These terms are not present in the standard linearised governing equations, see, for example, the analysis presented by Schmid and Henningson[19].

If the perturbations are assumed to have the normal mode form

$$(u, v, w, p) = [\hat{u}(y), \hat{v}(y), \hat{w}(y), \hat{p}(y)]e^{i(\alpha x + \beta z - \omega t)},$$

7

then (3) reduces to the following system of coupled ODEs

$$\left\{ \frac{\alpha^2}{R} \begin{bmatrix} 1 & 0 & 0 & 0 \\ 0 & 1 & 0 & 0 \\ 0 & 0 & 1 & 0 \\ 0 & 0 & 0 & 0 \end{bmatrix} + i\alpha \begin{bmatrix} U & 0 & 0 & 1 \\ 0 & U & 0 & 0 \\ 0 & 0 & U & 0 \\ 1 & 0 & 0 & 0 \end{bmatrix} + \begin{bmatrix} \mathscr{S}_{+1} & \mathscr{D}U & 0 & 0 \\ 0 & \mathscr{S}_{-1} & 0 & \mathscr{D} \\ 0 & 0 & \mathscr{S}_0 & i\beta \\ 0 & \mathscr{D} & i\beta & 0 \end{bmatrix} \right\} \begin{bmatrix} \hat{u} \\ \hat{v} \\ \hat{w} \\ \hat{p} \end{bmatrix} = \begin{bmatrix} 0 \\ 0 \\ 0 \\ 0 \end{bmatrix}, \tag{4}$$

where $\mathscr{S}_n = (R^{-1}\beta^2 - i\omega) + R^{-1}(V\mathscr{D} - \mathscr{D}^2) + nR^{-1}U$, and $\mathscr{D} = d/dy$. In our spectral analysis we assume that the frequency of the disturbance ω, and the spanwise wavenumber β, are solely real whilst the streamwise wavenumber α, is assumed to be complex $\alpha = \alpha_r + i\alpha_i$. As such, disturbances will grow exponentially in space when $\alpha_i < 0$.

Combining the governing equations together gives an Orr-Sommerfeld-type equation for this problem

$$(\mathscr{D}^2 - \gamma^2)^2\hat{v} - i\alpha R[(U - c)(\mathscr{D}^2 - \gamma^2)\hat{v} - \hat{v}\mathscr{D}^2 U] = V(\mathscr{D}^2 - \gamma^2)\mathscr{D}\hat{v} - U(\mathscr{D} - \gamma^2)\hat{v} + i\beta\mathscr{D}(U\hat{w}), \tag{5}$$

where $\gamma^2 = \alpha^2 + \beta^2$, and $c = \omega/\alpha$. The terms on the right-hand side are due to the influence of the surface stretching and do not normally appear in the standard Orr-Sommerfeld equation. The appearance of the spanwise wavenumber in (5) means that it is not possible to ensure that Squire's theorem will hold in this case. As such, it will be necessary to investigate both 3D and 2D modes in this study.

Given that the perturbation velocities are subject to the no-slip condition at the wall, and that all perturbations must decay to zero far from the surface, (4) is solved subject to

$$\hat{u}(y = 0) = \hat{v}(y = 0) = \hat{v}'(y = 0) = \hat{w}(y = 0) = 0,$$

$$\hat{u}(y \to \infty) \to \hat{v}(y \to \infty) \to \hat{w}(y \to \infty) \to \hat{p}(y \to \infty) \to 0. \tag{6}$$

The condition on the derivative of the wall-normal perturbation at $y = 0$, is simply a consequence of the form of the continuity equation.

B.   Numerical Method and Validation

The system of linear ODEs (4) is solved subject to the above boundary conditions (6) using a spectral method that utilises Chebyshev polynomials. These polynomials are defined like so

$$T_n(Y_j) = \cos[n \arccos(Y_j)], \quad n = 0, 1, 2, \ldots, N-1, N,$$

where N is the number of collocation points and the Gauss-Lobatto points Y_j, are defined as such

$$Y_j = -\cos\left(\frac{j\pi}{N}\right), \quad j = 0, 1, 2, \ldots, N-1, N.$$

In order to map the physical domain $0 \le y_j \le y_{max}$, to the computational domain $-1 \le Y_j \le +1$, the following exponential map is used

$$y_j = -\frac{1}{\phi} \ln\left(\frac{1 + Y_j + A}{A}\right),$$

where $A = 2(e^{-\phi y_{max}} - 1)^{-1}$, and ϕ is a free constant. In order to capture the exponential nature of the base flow a range of different ϕ values were tested (see Fig. 2 (a)). Our analysis revealed that choosing too large a value for ϕ resulted in solutions that did not converge within a desired tolerance, typically $\mathcal{O}(10^{-5})$. This was true irrespective of the choice of y_{max}, as the number of collocation points were increased. Too small a value for ϕ and the map reverted to a linear approximation, and was therefore unable to capture the exponential decay of the base flow solutions. A more moderate value of the constant, $\phi = 1/5$, proved to be a sensible choice, providing fully converged solutions when $y_{max} = 40$, and $N = 100$. It was somewhat surprising to note the requirement of such a large value for y_{max}, in order to obtain accurate numerical solutions. Many corresponding flat plate boundary-layer studies find that converged eigensolutions are obtained when the value of y_{max} is of the order of 20, for example Miller et al.[20]. However, we note that Davis and Pozrikidis[17] arrived at a similar conclusion when conducting their Görtler disturbance analysis.

In order to validate our numerical scheme it was tested against the results of Davis and Pozrikidis[17]. The authors showed, rather remarkably, that in the limit as $y \to \infty$, a simple relationship exists between the growth rate λ^*, and transverse wavenumber k^*, when searching for Görtler-type disturbances

$$\frac{\lambda^*}{\xi^*} = -(L^* k^*)^2 - \frac{1}{4}. \tag{7}$$

Our spectral scheme, which requires solving a quadratic eigenvalue problem, was used to solve their systems of ODEs subject to the standard conditions of no-slip and no-penetration at the wall and decay in to the far-field. We were able to exactly reproduce the results quoted by the authors,
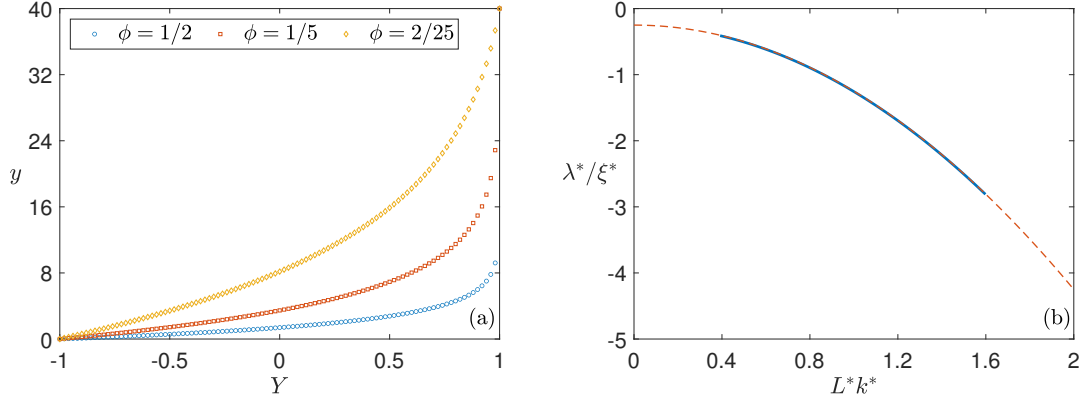
FIG. 2. In (a) the physical domain is mapped to the computational domain for a range of different ϕ values. In this study we use the value $\phi = 1/5$ for all quoted results. In (b) we reproduce the results of Davis and Pozrikidis[17]. Our numerical results, in the range $0.4 \leq L^*k^* \leq 1.6$, shown in blue, are plotted against the authors asymptotic prediction given in (7). The growth rate λ^*, is never greater than zero for any value of the transverse wavenumber k^*, and hence the flow is linearly stable to Görtler-type disturbances.

showing excellent agreement with both their asymptotic prediction and the results from their linear eigenvalue temporal analysis, see Fig. 2 (b).

C. Derivation of energy balance equations

In order to derive an appropriate integral energy analysis for this problem we take a linear combination of the constituent parts of (3b), average over one time period and integrate across the boundary layer. Having done so we arrive at the governing integral energy equation for flows of this nature

$$
\int_0^\infty \left[U \frac{\partial \mathscr{E}}{\partial x} + \frac{\partial (up)}{\partial x} - \frac{1}{R} \frac{\partial (v\Omega_z - w\Omega_y)}{\partial x} \right] \mathrm{d}y + \int_0^\infty \left[\frac{\partial (wp)}{\partial z} + \frac{1}{R} \frac{\partial (v\Omega_x - u\Omega_y)}{\partial z} \right] \mathrm{d}y
$$
$$
= -\int_0^\infty \left[\frac{U(2u^2 - \mathscr{E})}{R} + uv\mathscr{D}U \right] \mathrm{d}y - \int_0^\infty \frac{(\Omega_x^2 + \Omega_y^2 + \Omega_z^2)}{R} \mathrm{d}y,
$$

where $\mathscr{E} = (u^2 + v^2 + w^2)/2$, and Ω_i is the i-component of vorticity. Given that the perturbations have the normal mode form then it is possible to show that
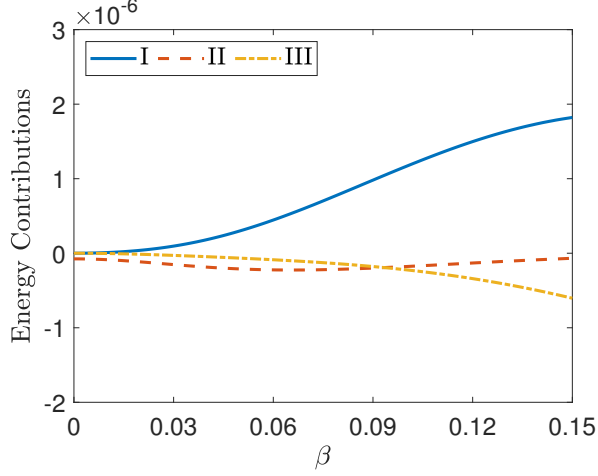
10

FIG. 3. Variation of the three energy contribution terms highlighted in (8) with the spanwise wavenumber β. For each value of β, the most unstable eigenmode ($\alpha_i = \max(\alpha_i)$) is selected, and the integrals as defined in (8), are computed at a fixed Reynolds number of $R = 1 \times 10^5$. These terms have not been normalised but prove to be negligible and so are excluded from the integral energy analysis and the associated integral energy equation presented in (9).

$$-2\alpha_i \int_0^\infty \left(U\langle\hat{\mathscr{E}}\rangle + \langle\hat{u}\hat{p}\rangle + \overbrace{\frac{\beta\langle\hat{u}\hat{w}\rangle}{R}}^{\text{I}} \right) \mathrm{d}y = -\int_0^\infty \left[\frac{U(2\langle\hat{u}^2\rangle - \langle\hat{\mathscr{E}}\rangle)}{R} + \langle\hat{u}\hat{v}\rangle\mathscr{D}U \right] \mathrm{d}y$$
$$- \int_0^\infty \left[\frac{\langle\hat{u}'^2\rangle + \langle\hat{w}'^2\rangle}{R} + \underbrace{\frac{(\alpha_r^2 - \alpha_i^2)(\langle\hat{v}^2\rangle + \langle\hat{w}^2\rangle)}{R}}_{\text{II}} + \underbrace{\frac{\beta^2(\langle\hat{u}^2\rangle + \langle\hat{v}^2\rangle)}{R}}_{\text{III}} \right] \mathrm{d}y, \quad (8)$$

where $\langle\hat{\mathscr{E}}\rangle = (\langle\hat{u}^2\rangle + \langle\hat{v}^2\rangle + \langle\hat{w}^2\rangle)/2$, and $\langle\hat{x}\hat{y}\rangle = \hat{x}^\star\hat{y} + \hat{x}\hat{y}^\star$, with * indicating the complex conjugate. The first term on the right-hand side of (8) exists solely due to the influence of the surface stretching. The second is the 'standard' Reynolds stress term that appears in all 2D and 3D analyses of this type (see, for example, Porter[21]). All the terms included in the final integral term are associated with the action of viscous dissipation.

Our numerical investigations reveal that for all the cases considered here, terms I − III (highlighted above) are in fact negligible, with their absolute value always being less than 2×10^{-6} (see Fig. 3). It transpires that the above integral energy equation can be approximated like so

$$\underbrace{-2\alpha_i}_{\text{TME}} \simeq \underbrace{-\int_0^\infty \langle\hat{u}\hat{v}\rangle\mathscr{D}U \, \mathrm{d}y}_{\text{EPRS}} - \underbrace{\int_0^\infty \frac{U(2\langle\hat{u}^2\rangle - \langle\hat{\mathscr{E}}\rangle)}{R} \, \mathrm{d}y}_{\text{EDSS}} - \underbrace{\int_0^\infty \frac{\langle\hat{u}'^2\rangle + \langle\hat{w}'^2\rangle}{R} \, \mathrm{d}y}_{\text{EDV}}, \quad (9)$$

11

TABLE I. Critical values (indicated by the superscript 'crit') for the frequency, streamwise wavenumber and Reynolds number for a range of fixed values of the spanwise wavenumber, β. The critical values of ω and α_r are given to four decimal places whilst the critical Reynolds number is quoted accurate to five significant figures.

β	ω^{crit}	α_r^{crit}	R^{crit}
0	0.1364	0.1614	48499.1
0.05	0.1310	0.1550	50911.5
0.1	0.1139	0.1348	60652.0
0.15	0.0823	0.0971	96607.5

where the right-hand side of (9) has been normalised by the integral of the combination of energy flux and the work done by the pressure, $\mathcal{N} = \int_0^\infty (U\langle\hat{\mathscr{E}}\rangle + \langle\hat{u}\hat{p}\rangle)\,dy$. The energy production term, labelled EPRS− **E**nergy **P**roduction due to **R**eynolds **S**tresses, will always be positive and the dissipation terms, labelled EDSS− **E**nergy **D**issipation due to **S**urface **S**tretching and EDV− **E**nergy **D**issipation due to **V**iscosity, will always be negative. Therefore, in the cases when the production is greater than the absolute value of the dissipation, the right-hand side of (9) will be greater than zero. In these cases the eigenmode in question is amplified and the **T**otal **M**echanical **E**nergy of the system is positive. Clearly, this can only hold true if $\alpha_i < 0$, which is consistent with our definition of linear instability.

III. NUMERICAL RESULTS

Having validated our numerical scheme we begin by solving (4) subject to (6) for fixed values of β whilst cycling through a range of values of ω and R in order to determine points where $\alpha_i \leq 0$. A point is deemed to be neutrally stable if $\alpha_i = 0$. When considering 2D perturbations only ($\beta = 0$) we find that the flow is linearly unstable above a critical Reynolds number of $R^{\text{crit}} = 48,499$ (see Table I). Although this critical Reynolds number is large when compared to a Blasius-type boundary-layer flow, these results do clearly show that this flow is susceptible to instabilities arising from travelling-wave disturbances. In fact, the critical Reynolds number noted above, is of the same order of that exhibited by other boundary-layer flows with exponentially decaying base flow solutions, for example, the asymptotic suction boundary-layer flow which has a critical
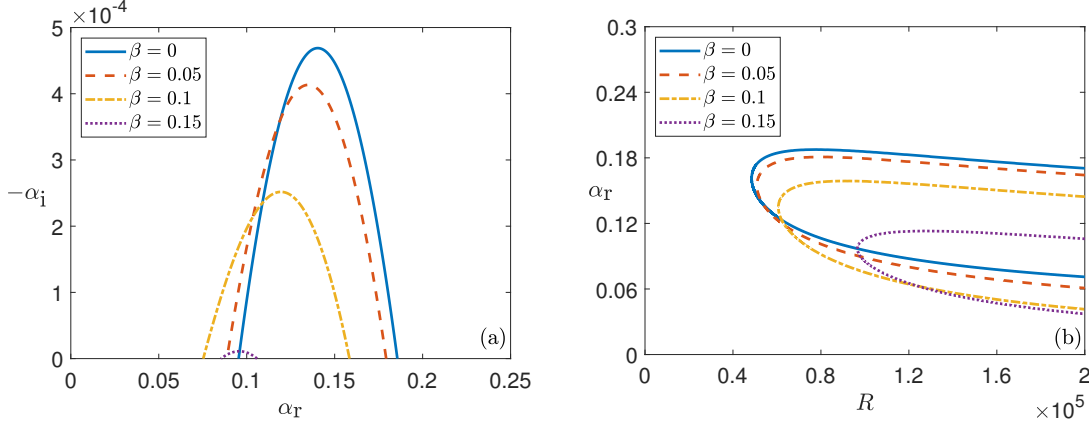
FIG. 4. In (a) the growth rate, defined as $-\alpha_i$, is plotted against α_r, for a range of β values at a fixed value of the Reynolds number, $R = 1 \times 10^5$. In (b) the curves of neutral stability, all the points where $\alpha_i = 0$, are plotted for the same range of β values. As the value of the spanwise wavenumber increases the area encompassed by the curve is reduced.

Reynolds number, as quoted by Dempsey and Walton[22], of $R^{\mathrm{crit}} \simeq 54,370$.

Although an equivalent to Squire's theorem cannot be proved for this type of flow we do find that two-dimensional disturbances are indeed the most unstable. Fig. 4 (a) presents a snapshot of the linear growth rates for a range of β values at a fixed Reynolds number, $R = 1 \times 10^5$. We find that the amplitude of the growth rate is significantly reduced as β increases. This observed stabilisation is further exemplified by the neutral stability curves for α_r presented in Fig. 4 (b), showing that the critical Reynolds number increases as the spanwise wavenumber increases. In addition to this, the area encompassed by the neutral curves is also reduced. Physically, this means that there are fewer wavenumbers that are susceptible to linear instability.

We find that as the value of the spanwise wavenumber is increased above even moderate values, $\beta \gtrsim 0.187$, the flow becomes linearly stable. This suggests that in the cases when β is greater than this value the area encompassed by the neutral stability curve becomes vanishingly small, and thus, the critical Reynolds number asymptotes towards positive infinity. Given that we were unable to categorically prove that 3D disturbances would be more stable than 2D disturbances, due to the additional terms appearing in the modified Orr-Sommerfeld equation (5), these numerical results provide strong evidence that this must indeed be the case.

Before discussing our results associated with the integral energy analysis derived in II C it proves useful to first determine the form of each of the three eigenfunctions. In Fig. 5 (a), Fig. 5 (b)
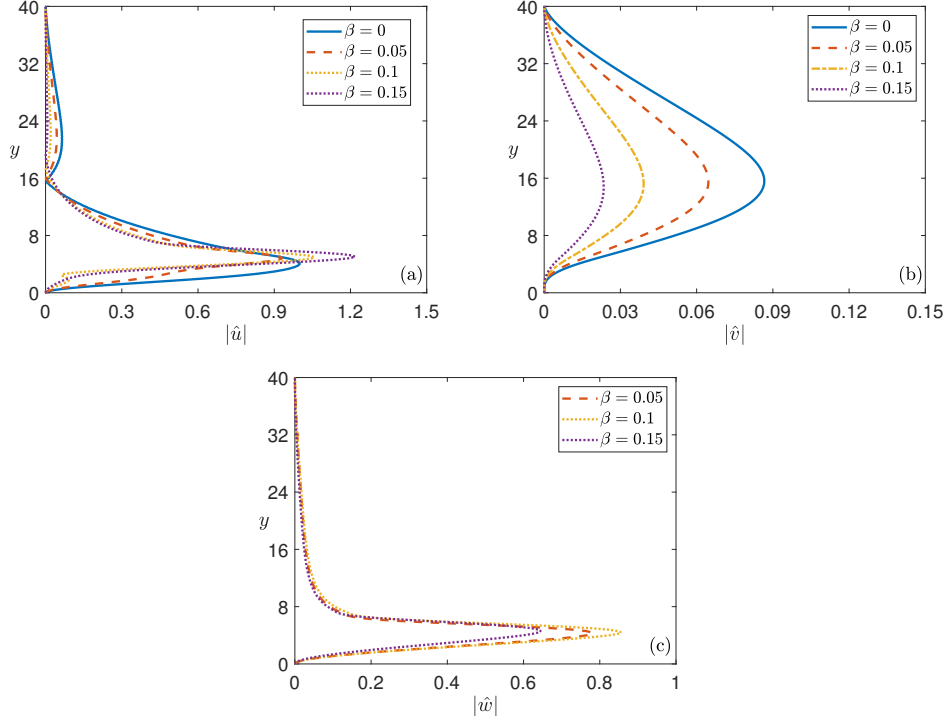
FIG. 5. Plots of the streamwise, wall-normal and spanwise eigenfuncions for a range of β values at a fixed value of the Reynolds number, $R = 1 \times 10^5$. In each case the most unstable eigenmode ($\alpha_i = \max(\alpha_i)$) is selected. All the results have been normalised with respect to the maximum value of $|\hat{u}|$ for the case when $\beta = 0$.

and Fig. 5 (c) we present plots of $|\hat{u}|$, $|\hat{v}|$ and $|\hat{w}|$ for a range of spanwise wavenumbers. As the value of β increases we observe that the streamwise eigenfunctions decay to zero closer to the boundary-layer wall, providing supporting evidence for the observed stabilisation. In addition to this, we also notice that the peak of the wall-normal eigenfunction is also notably reduced. Whilst these eigenfunctions do decay to zero in a region close to $y = y_{\max}$, suitable numerical testing has taken place to ensure that these results are indeed independent of our numerical scheme. With regards to the spanwise eigenfunction, no such clear and obvious trends appear to exist. In fact, it would appear that there exists some β in the range $0.05 < \beta < 0.15$ such that the value of $\max|\hat{w}|$, is itself maximised. This suggests that the energy production and dissipation terms associated with this system will not increase and decrease linearly as the value of the spanwise wavenumber is increased.

In Fig. 6 we then plot the functions associated with the energy production due to Reynolds stresses, and the energy dissipation due to surface stretching and viscosity, for a range of β values
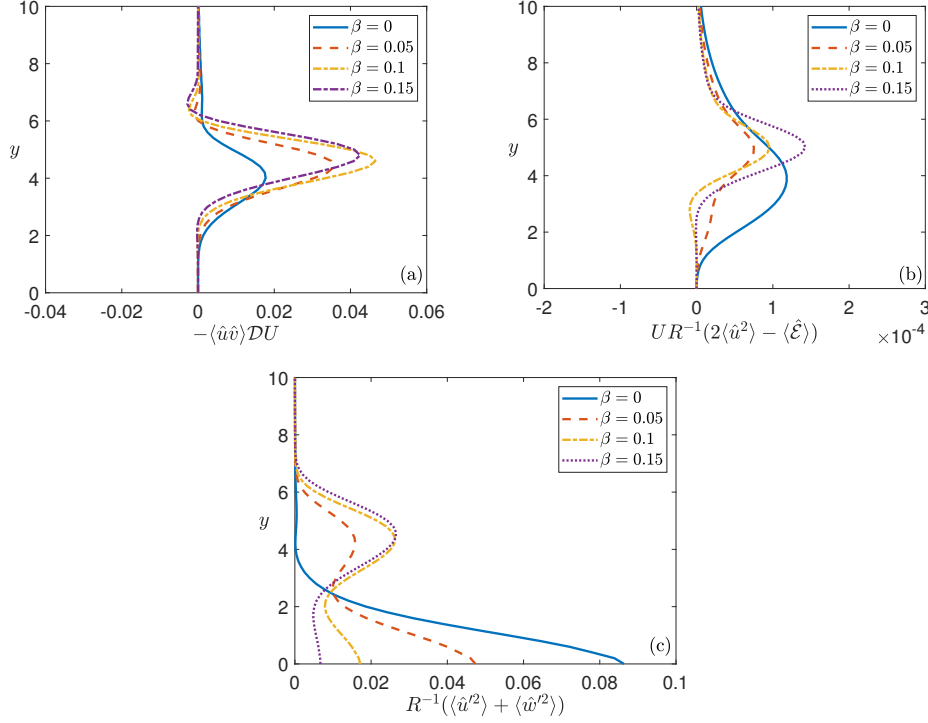
14

FIG. 6. Plots of the functions associated with the Energy Production due to Reynolds Stresses in (a), the Energy Dissipation due to Surface Stretching in (b), and the Energy Dissipation due to Viscosity in (c). It should be noted that in (c), in the case when $\beta = 0$, the plot depends only on $\hat{u}'$ and R, since $\hat{w}' \equiv 0$. As before, the value of the Reynolds number is fixed at $R = 1 \times 10^5$, and the most unstable eigenmode is selected.

in order to determine their relative influence on the normalised energy balance. We observe in Fig. 6 (a) that the area encompassed by the energy production curves initially increases as the value of β increases. However, in much the same way as before, we notice that the peak of the curve eventually decreases as a function of the spanwise wavenumber. This suggests that there exists a critical value of the spanwise wavenumber, whereby, above this critical value, the contribution of energy production due to Reynolds stresses begins to decrease. It is clear from Fig. 6 (b) that the contribution of energy dissipation from the terms associated with surface stretching are minimal. These terms are much larger in magnitude than those ignored in II C, however, they are still roughly two orders of magnitude smaller than the dissipation term associated with the action of viscosity. It is therefore clear, from this figure, that the additional terms appearing in (5) play a very minimal role in the overall energetics of the system. This suggests that the linear stability of the flow is primarily governed by the form of the base flow and the standard Orr-Sommerfeld equation. It is
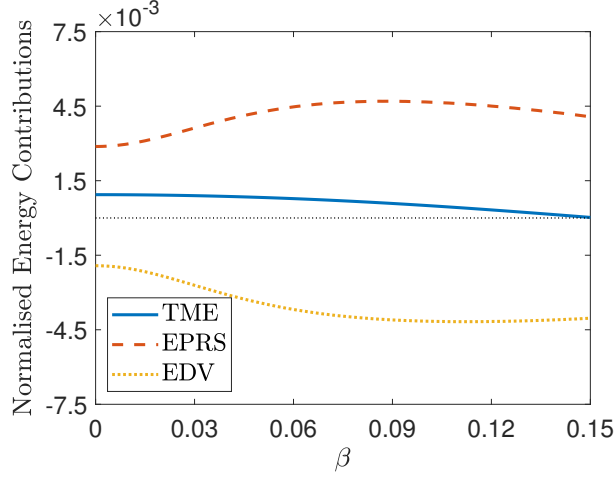
FIG. 7. A plot of the variation of the Total Mechanical Energy (TME), the Energy Production due to Reynolds Stresses (EPRS) and the Energy Dissipation due to Viscosity (EDV) against the spanwise wavenumber. The point at which the flow transitions from linearly unstable to linearly stable is indicated here by the dotted black line. For all the β values presented here the flow is linearly unstable.

clear, from Fig. 6 (c), that the energy dissipation functions associated with the action of viscosity decay to zero farther from the boundary-layer wall as the spanwise wavenumber is increased. This would suggest that the absolute value of the energy dissipation term will likely increase with β.

In Fig. 7 the normalised energy contributions, as defined in (9), are presented for increasing values of the spanwise wavenumber. Note that here we exclude the contribution from the EDSS terms as these have now been shown to be negligible in this context. As predicted by our prior analysis the energy production initially increases before levelling off and eventually decreasing. The absolute value of the energy dissipation due to viscosity follows a similar trend and, as such, the total mechanical energy of the system decreases with increasing β. This result is entirely consistent with the conclusions drawn from our neutral stability curve predictions.

IV. LARGE REYNOLDS NUMBER ASYMPTOTIC ANALYSIS

In order to investigate the structure of the TS waves in the near-wall viscous layer we now present a large Reynolds number lower branch asymptotic stability analysis. The most amplified TS disturbances appear near to the lower branch of the neutral curve and this, along with the need to validate our numerical solutions, provides the motivation for the lower rather than the upper branch analysis.

We analyse the Orr-Sommerfeld-type equation (5) in the limit as $R \to \infty$, for neutrally stable solutions. Initially, we focus on two-dimensional disturbances ($\beta = 0$), so to leading order this becomes Rayleigh's equation, namely

$$(U - c)(\mathscr{D}^2 - \alpha^2)\hat{v} - \hat{v}\mathscr{D}^2 U = 0.$$

We note that although (5) includes additional terms associated with surface stretching, in the limit as $R \to \infty$, we do recover the standardised version of Rayleigh's equation. This equation holds away from fixed walls and the critical layer (where $U = c$), since, in these regions, viscous effects cannot be ignored. In these regions, for $R \gg 1$, (5) becomes

$$\mathscr{D}^4 \hat{v} \approx i\alpha R(U - c)\mathscr{D}^2 \hat{v}. \tag{10}$$

Close to the wall, $U(y) \approx 1 - y + \cdots$, and we find from (10) that the thickness of the wall layer is $\mathscr{O}((\alpha R(1 - c))^{-1/2})$, where we note, from the numerical solutions, that $0 < c < 1$. The critical layer is located at $y = y_c$, say, where $U(y_c) = c$, i.e. where $e^{-y_c} = c$, yielding $y_c = -\ln c$. Analysis of (10) determines the thickness of the critical layer to be $\mathscr{O}((R\omega)^{-1/3})$. On the lower branch of the neutral stability curve, the wall layer and the critical layer merge, yielding $(1 - c) \sim (\alpha R)^{-1/3}$. In addition, the numerical solutions suggest that $(1 - c) \sim R^{-1/4}$, which leads to the scales $\alpha \sim \omega \sim R^{-1/4}$, on the lower branch of the neutral stability curve. For the case of three-dimensional disturbances $\beta \sim \alpha$, so $\beta \sim R^{-1/4}$, also.

For the ensuing asymptotic analysis it is convenient to non-dimensionalise lengths with respect to a reference length l^*, velocities with respect to $\xi^* l^*$, time with respect to $1/\xi^*$ and pressure with respect to $\rho^* \xi^{*2} l^{*2}$. Thus, we write $(x^*, y^*, z^*) = l^*(\bar{x}, \bar{y}, \bar{z})$, $(\tilde{U}^*, \tilde{V}^*, \tilde{W}^*) = \xi^* l^*(\overline{U}, \overline{V}, \overline{W})$, $t^* = \bar{t}/\xi^*$ and $\tilde{P}^* = \rho^* \xi^{*2} l^{*2} \overline{P}$. This leads to the definition of a Reynolds number $Re = \xi^* l^{*2}/\nu^*$. We perform a local stability analysis about the streamwise location $\bar{x}_s$ for $Re \gg 1$. The relationship between this Reynolds number and the local Reynolds number used in the numerical analysis is then $R = Re^{1/2}\bar{x}_s$. We will return to this relationship when comparing the asymptotic solutions with the numerical ones. Thus, in terms of Re, $(1 - c) \sim \alpha \sim \omega \sim Re^{-1/8}$.

The ratio of the length scales is $l^*/L^* = Re^{1/2}$ and similarly, the ratio of the time scales is $Re^{1/2}\bar{x}_s$. This gives the relations $(\bar{x}, \bar{y}, \bar{z}) = Re^{-1/2}(x, y, z)$ and $\bar{t} = Re^{-1/2}t/\bar{x}_s$. Then, in terms of Re, the streamwise and spanwise length scales and the timescale, are $\mathscr{O}(Re^{-3/8})$. Also, the thickness of the wall layer is $\mathscr{O}(Re^{-1/2}Re^{-1/8}) = \mathscr{O}(Re^{-5/8})$. We introduce scaled coordinates

and time to reflect these scales. For convenience, we set $\varepsilon = Re^{-1/8}$, and write

$$\bar{x} - \bar{x}_s = \varepsilon^3 X, \quad \bar{z} = \varepsilon^3 Z, \quad \text{and} \quad \bar{t} = \varepsilon^3 \tau.$$

Thus the non-dimensional disturbed flow is described as such

$$(\overline{U}, \overline{V}, \overline{W}, \overline{P}) = (\bar{x}U(y), Re^{-1/2}V(y), 0, Re^{-1}P(y)) + (\tilde{u}, \tilde{v}, \tilde{w}, \tilde{p}),$$

where the small disturbance quantities, denoted with a tilde, are functions of $\bar{x}, \bar{y}, \bar{z}$ and $\bar{t}$.

A. Triple-deck structure

Similarly to the instability analysis of the Blasius flow (uniform flow past a flat plate), we find we have a triple-deck structure, with upper, main and lower deck thicknesses of order $Re^{-3/8}$, $Re^{-1/2}$ and $Re^{-5/8}$, respectively. The analysis turns out to be similar to the corresponding case for a Blasius boundary layer (see Smith[23]), although with the notable difference that the timescale that the disturbances develop over is equal to the streamwise lengthscale. The main deck covers the extent of the boundary layer, where the disturbances are inviscid and rotational. The upper deck is inviscid and irrotational in nature and required to reduce the disturbances to zero in the far field. The lower deck is required to satisfy the viscous no-slip boundary conditions at the moving surface.

We consider normal-mode solutions and take the perturbations proportional to $E = \exp(i(\theta(X) + \overline{\beta}Z - \overline{\omega}\tau))$. Then the wavenumber θ, is a slowly varying function of $\bar{x}$ in the form

$$\frac{\mathrm{d}\theta}{\mathrm{d}X} = \overline{\alpha} = \alpha_0(\bar{x}) + \varepsilon\alpha_1(\bar{x}) + \cdots.$$

The spanwise wavenumber $\overline{\beta}$ and the frequency $\overline{\omega}$ are constant and expand as $\overline{\beta} = \beta_0 + \varepsilon\beta_1 + \cdots$, and $\overline{\omega} = \omega_0 + \varepsilon\omega_1 + \cdots$. We begin our analysis in the main deck where $\bar{y} = Re^{-1/2}y = \varepsilon^4 y$, and the disturbances expand as

$$\tilde{u} = (U_{m0} + \varepsilon U_{m1} + \cdots)E,$$
$$\tilde{v} = (\varepsilon V_{m0} + \varepsilon^2 V_{m1} + \cdots)E,$$
$$\tilde{w} = (\varepsilon W_{m0} + \varepsilon^2 W_{m1} + \cdots)E,$$
$$\tilde{p} = (\varepsilon P_{m0} + \varepsilon^2 P_{m1} + \cdots)E,$$

18

where $U_{m0},\ldots,V_{m0},\ldots,W_{m0},\ldots,$ and $P_{m0}\ldots,$ are functions of y and the slow variable $\bar{x}$. We substitute this form for the disturbance quantities into the linear perturbation equations and equate leading order terms. We find that the solutions for the leading-order velocity and pressure disturbances are

$$U_{m0} = -B_0(\bar{x})U'(y), \tag{11a}$$

$$V_{m0} = i\frac{B_0(\bar{x})}{\bar{x}_s}(\alpha_0\bar{x}_sU(y) - \omega_0), \tag{11b}$$

$$W_{m0} = -\frac{\beta_0 P_{m0}(\bar{x})}{\alpha_0\bar{x}_sU(y) - \omega_0}, \tag{11c}$$

$$P_{m0} = P_{m0}(\bar{x}), \tag{11d}$$

where $P_{m0}(\bar{x})$ and $B_0(\bar{x})$ are unknown, slowly varying, amplitude functions (representing pressure and negative displacement perturbations, respectively). For these viscous instability modes we choose

$$\alpha_0\bar{x}_s = \omega_0.$$

This corresponds to the critical layer, where $U = \overline{\omega}/(\overline{\alpha}\bar{x}_s)$, moving to the wall at leading order. An outer layer (the upper deck) is then required to reduce the disturbances to zero as $y \to \infty$.

In the upper deck $\bar{y} = \varepsilon^3\tilde{y}$, with $\tilde{y} = \mathcal{O}(1)$. Of interest here is the matching of the normal velocities between the upper and the main deck. Here

$$\tilde{v} = (\varepsilon\overline{V}_0 + \varepsilon^2\overline{V}_1 + \cdots)E,$$

and similarly for $\tilde{u}$, $\tilde{w}$ and $\tilde{p}$. In the upper deck the basic flow has the behaviour $U \to 0$, and $V \to -1$. The solution for $\overline{V}_0$ is found to be

$$\overline{V}_0 = i\frac{(\alpha_0^2 + \beta_0^2)^{1/2}}{\alpha_0\bar{x}_s}P_{m0}(\bar{x})e^{-(\alpha_0^2+\beta_0^2)^{1/2}\tilde{y}}.$$

Matching $\overline{V}_0$ as $\tilde{y} \to 0$, with V_{m0} as $y \to \infty$, yields the relation

$$B_0(\bar{x}) = -\frac{(\alpha_0^2 + \beta_0^2)^{1/2}}{\alpha_0^2\bar{x}_s}P_{m0}(\bar{x}). \tag{12}$$

The desired dispersion relation is obtained by matching the solutions in the main deck with those in the lower deck, which is examined next.

In the lower deck $\bar{y} = \varepsilon^5 \overline{Y}$, with $\overline{Y} = \mathcal{O}(1)$. Close to the wall $U \approx 1 - \varepsilon \overline{Y} + \cdots$ and $V \approx -\varepsilon \overline{Y} + \cdots$. Then, to match with the main deck solutions, the disturbance quantities expand as

$$\tilde{u} = (U_0 + \varepsilon U_1 + \cdots)E,$$
$$\tilde{v} = (\varepsilon^2 V_0 + \varepsilon^3 V_1 + \cdots)E,$$
$$\tilde{w} = (W_0 + \varepsilon W_1 + \cdots)E,$$
$$\tilde{p} = (\varepsilon P_0 + \varepsilon^2 P_1 + \cdots)E,$$

where $U_0, \ldots, V_0, \ldots, W_0, \ldots$, and $P_0, \ldots$ depend on $\overline{Y}$ and $\bar{x}$.

Leading order terms in the y-momentum equation yield $P_0 = P_{m0}$. The remaining equations show that $\alpha_0 U_{0\overline{Y}} + \beta_0 W_{0\overline{Y}}$, satisfies Airy's equation, namely,

$$(\alpha_0 U_{0\overline{Y}} + \beta_0 W_{0\overline{Y}})_{\overline{Y}\overline{Y}} - (\mathrm{i}(\alpha_1 \bar{x}_s - \omega_1) - \mathrm{i}\alpha_0 \bar{x}_s \overline{Y})(\alpha_0 U_{0\overline{Y}} + \beta_0 W_{0\overline{Y}}) = 0, \tag{13}$$

where here the subscript $\overline{Y}$ denotes differentiation with respect to $\overline{Y}$. The solution for U_0 must satisfy

$$U_0(\overline{Y} = 0) = 0, \quad U_0(\overline{Y} \to \infty) \to -\frac{(\alpha_0^2 + \beta_0^2)^{1/2}}{\alpha_0^2 \bar{x}_s} P_{m0}.$$

By setting

$$\zeta = (-\mathrm{i}\alpha_0 \bar{x}_s)^{1/3} \left(\overline{Y} - \frac{\alpha_1 \bar{x}_s - \omega_1}{\alpha_0 \bar{x}_s} \right),$$

then the solution of (13), which is bounded as $\zeta \to \infty$, is

$$\alpha_0 U_{0\zeta} + \beta_0 W_{0\zeta} = C_0 \mathrm{Ai}(\zeta),$$

where Ai is the (appropriately decaying) Airy function and the subscript ζ denotes differentiation with respect to ζ. Integrating the above and satisfying the boundary conditions $U_0(\zeta = \zeta_0) = W_0(\zeta = \zeta_0) = 0$, yields

$$\alpha_0 U_0 + \beta_0 W_0 = C_0 \int_{\zeta_0}^{\zeta} \mathrm{Ai}(\bar{\zeta}) \, \mathrm{d}\bar{\zeta},$$

where

$$\zeta_0 = e^{i5\pi/6}(\alpha_0 \bar{x}_s)^{-2/3}(\alpha_1 \bar{x}_s - \omega_1).$$

Applying the boundary conditions $U_0(\overline{Y} = 0) = V_0(\overline{Y} = 0) = 0$, in the leading-order y- and z-momentum equations yields

$$U_{0\overline{YY}}(\overline{Y} = 0) - i\alpha_0 P_0 = W_{0\overline{YY}}(\overline{Y} = 0) - i\beta_0 P_0 = 0.$$

Thus, we determine the following relation between C_0 and P_{m0}

$$(-i\alpha_0 \bar{x}_s)^{2/3} C_0 \text{Ai}'(\zeta_0) = i(\alpha_0^2 + \beta_0^2)P_{m0}. \tag{14}$$

B. Eigenrelation

Matching $\alpha_0 U_0 + \beta_0 W_0$ between the main and lower decks, using (12), gives a second relation between C_0 and P_{m0}

$$C_0 \int_{\zeta_0}^{\infty} \text{Ai}(\zeta)\,d\zeta = -\frac{(\alpha_0^2 + \beta_0^2)^{1/2}}{\alpha_0 \bar{x}_s}P_{m0}. \tag{15}$$

Combining (14) and (15) yields the desired eigenrelation

$$\text{Ai}'(\zeta_0) = \kappa(-i\alpha_0 \bar{x}_s)^{1/3}(\alpha_0^2 + \beta_0^2)^{1/2}, \tag{16}$$

where $\kappa = \int_{\zeta_0}^{\infty} \text{Ai}(\zeta)\,d\zeta$. It is possible to scale $\bar{x}_s$ from the above eigenrelation by writing

$$(\alpha_0, \beta_0) = \bar{x}_s^{-1/4}(\overline{\alpha}_0, \overline{\beta}_0), \quad \text{and} \quad \alpha_1 \bar{x}_s - \omega_1 = \bar{x}_s^{1/2}\overline{\gamma}_1.$$

The eigenrelation (16) then becomes

$$\text{Ai}'(\zeta_0) = \kappa e^{-i\pi/6}\overline{\alpha}_0^{1/3}(\overline{\alpha}_0^2 + \overline{\beta}_0^2)^{1/2}, \tag{17}$$

where $\zeta_0 = e^{i5\pi/6}\overline{\alpha}_0^{-2/3}\overline{\gamma}_1$.

This eigenrelation can be expressed in terms of the Tietjens function (see, for example, Reid[24]). Using the notation in Healey[25] this function is given as

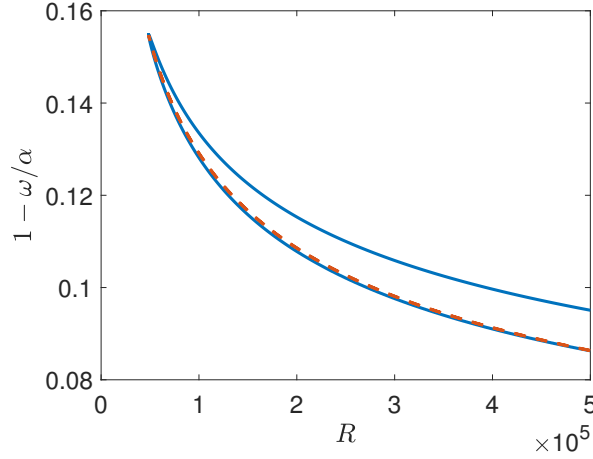$$F^+(\xi_0) = 1 - \frac{\text{Ai}'(\xi_0)}{\xi_0 \int_{\infty}^{\xi_0} \text{Ai}(\xi)\,d\xi},$$

FIG. 8. Comparison of the asymptotic approximation $1 - \omega/\alpha \approx 2.296R^{-1/4}$, with our numerical result in the case when $\overline{\beta}_0 = \beta = 0$. The solid line represents the curve of neutral stability for two-dimensional disturbances. The dashed line is the lower branch asymptotic solution.

where $\xi_0 = e^{-i5\pi/6}z$. For our problem of the stability of the flow due to a linear stretching sheet, the eigenrelation (17) becomes

$$F^+(\zeta_0) - 1 = -\frac{\overline{\alpha}_0}{\overline{\gamma}_1}(\overline{\alpha}_0^2 + \overline{\beta}_0^2)^{1/2}. \tag{18}$$

Restricting our attention to neutrally stable solutions ($\overline{\alpha}_0$ real), since ζ_0 is the complex conjugate of ξ_0, inspection reveals that $F^+(\zeta_0)$ is the complex conjugate of $F^+(\xi_0)$. A well-known property of the Tietjens function $F^+(e^{-i5\pi/6}z)$ is that it is real for $z = z_0 \approx 2.297$, with $F^+(e^{-i5\pi/6}z_0) \approx 0.564$. In relation to the instability of the Blasius boundary layer, $z = z_0$ corresponds to the lower branch of the neutral stability curve, while $F^+(\xi_0) \to 0$, as $|\xi_0| \to \infty$, and this limit is relevant to the upper branch (Healey[25]). Thus, approximations to the neutral solutions of (18) for two-dimensional disturbances can be obtained easily, yielding $\overline{\alpha}_0 \approx 1.001$, and $\overline{\gamma}_1 \approx 2.299$. These values are confirmed by numerical solution of (18).

In order to compare the asymptotic predictions with the numerical solutions obtained in III we consider an asymptotic expansion in terms of $c = \omega/\alpha$. We have that

$$1 - \frac{\omega}{\alpha} = 1 - \frac{\overline{\omega}}{\overline{\alpha}\overline{x}_s} = \varepsilon\frac{\alpha_1\overline{x}_s - \omega_1}{\alpha_0\overline{x}_s} + \cdots = R^{-1/4}\frac{\overline{\gamma}_1}{\overline{\alpha}_0} + \cdots. \tag{19}$$

Thus, for $\overline{\beta}_0 = 0$, this gives the approximation $1 - \omega/\alpha \approx 2.296R^{-1/4}$. This is compared with the numerical solution from III in Fig. 8, showing excellent agreement. Solutions of (18) can also be
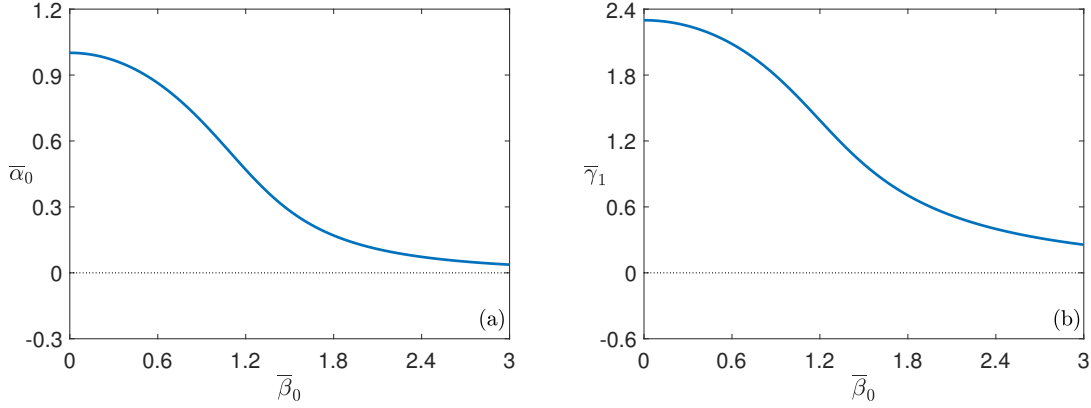
22

FIG. 9. Plots of the neutral solutions of (18) for a range of $\overline{\beta}_0$ values. In (a) and (b) we plot $\overline{\alpha}_0$ and $\overline{\gamma}_1$ against $\overline{\beta}_0$, respectively.

obtained numerically for $\overline{\beta}_0 \neq 0$. The neutral values of $\overline{\alpha}_0$ and $\overline{\gamma}_1$ obtained for a range of values of $\overline{\beta}_0$ are shown in Fig. 9. The first term in the approximation of $R^{1/4}(1 - \omega/\alpha) = \overline{\gamma}_1/\overline{\alpha}_0$, can then be inferred for a range of values of $\overline{\beta}_0$.

In order to compare the three-dimensional results with the computational results we use the relation $\beta = R^{-1/4}\overline{\beta}_0$ at leading order. Then the asymptotic solution for a fixed value of $\overline{\beta}_0$ can be compared with the computational solution for three-dimensional modes where β is given as above. For each value of R the value of β is determined and the neutral values of α and ω are determined (a similar comparison is made for the asymptotic suction boundary layer by Dempsey and Walton[22] in their Fig. 3). In Fig. 10 we plot such comparisons for the cases when $\overline{\beta}_0 = 1/2$, and $\overline{\beta}_0 = 1$. As before excellent agreement can be seen between the one-term asymptotic result and lower branch of the numerically calculated neutral stability curve.

V.   DISCUSSION AND CONCLUSIONS

We have assessed the onset of instability of the flow due to a linear stretching sheet. Previous studies, which consider only Görtler-type disturbances, have concluded that this flow is linearly stable. However, our analysis has revealed that this flow is susceptible to disturbances in the form of Tollmien-Schlichting waves.

The flow itself is a rare example of an exact analytical solution of the Navier-Stokes equations. Our analyses, both numerical and analytical, reveal that this flow is linearly unstable to travelling wave disturbances. Although we have been unable to rigorously prove an equivalent to Squire's
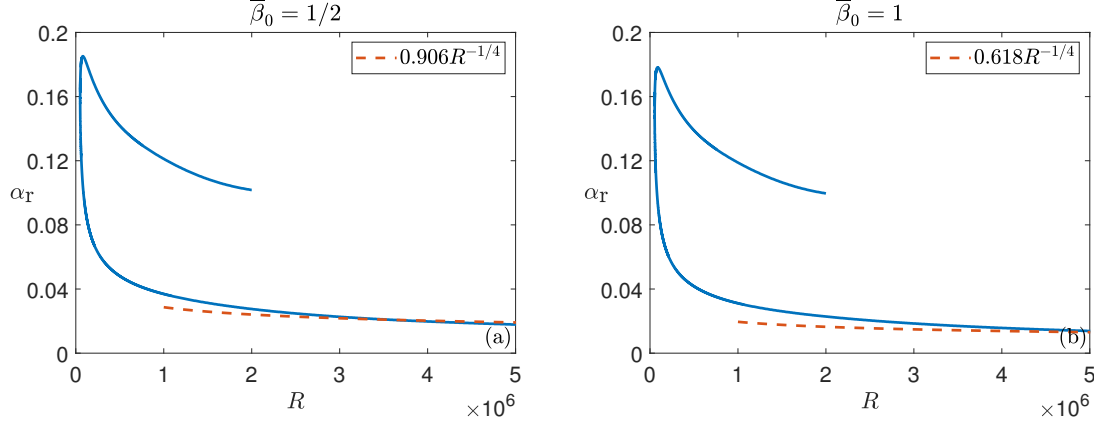
23

FIG. 10. Comparison between the three-dimensional asymptotic solutions and the corresponding curves of neutral stability. The results for the cases when $\overline{\beta}_0 = 1/2$, and $\overline{\beta}_0 = 1$ are plotted in (a) and (b), respectively. At each step in the numerical solution procedure the value of the spanwise wavenumber is updated according to the relation $\beta = R^{-1/4}\overline{\beta}_0$. The upper branch of the neutral stability curve has been truncated at $R = 2 \times 10^6$.

theorem for this type of flat plate boundary-layer flow we have shown numerically that 2D disturbances are indeed the most unstable. In this case, the critical Reynolds number is of the same order as other flat plate flows exhibiting exponentially decaying base flow solutions.

Our integral energy analysis reveals that the total mechanical energy of the system will always decrease as the spanwise wavenumber increases. This result aligns with the fact that the critical Reynolds number increases (with associated decreasing growth rates) as the value of β increases from zero. Given that the streamwise velocity component is x-dependent and that the wall-normal velocity component is non-zero, a number of additional terms appear in a governing Orr-Sommerfeld-type equation. However, these terms are all of order $\mathscr{O}(R^{-1})$, and, as evidenced by our integral energy analysis, therefore play a negligible role in the linear stability characteristics of this system.

The large Reynolds number asymptotic analysis presented in IV produces excellent results when compared to our numerical solutions. Of particular note is the exceptional agreement observed between the two sets of solutions in the most unstable case when $\overline{\beta}_0 = \beta = 0$.

Given that for this type of flow, the local Reynolds number R is directly related to the streamwise location at which the stability analysis is applied, one can infer the dimensional lengthscale associated with the onset of linear instability given that the critical Reynolds number, stretching

rate and kinematic viscosity are known

$$x_s^* = R \frac{v^*}{\xi^* L^*} = R \sqrt{\frac{v^*}{\xi^*}}.$$

Given the critical Reynolds number results presented here, with a fluid of kinematic viscosity $v^* = 1 \times 10^{-6}\,\mathrm{m^2 s^{-1}}$, and a dimensional stretching rate of $\xi^* = 20\,\mathrm{s^{-1}}$ (as is consistent with the analysis of Vleggaar[3], in fact, this estimate for ξ^* is likely to be very conservative given the data presented in Fig. 1 of Vleggaar's study), the onset of linear instability for a flow involving the cooling of a continuously extended sheet would be predicted to be of the order of $x_s^* = \mathcal{O}(10^1)\,\mathrm{m}$. As such, the possibility of this type of instability being realised in an industrial context are perhaps somewhat limited. However, in order to be able to more accurately model industrial processes involving surface stretching a number of additional considerations should be taken in to account. Including the effects of a large temperature gradient on the flow of a polymeric fluid would result in a modification of not only the base flow profiles but also the governing perturbation equations (as evidenced in related studies by Miller *et al.*[20] and Cracco, Davies, and Phillips[26], for example). This, in turn, would affect the predictions for the critical Reynolds number for the onset of linear instability. Combining this with the fact that the intrinsic properties of the fluid would also be changing, could result in a significantly reduced prediction for x_s^*. Indeed, this will be the goal of the continuation of this study. Using the framework developed here we plan to include the above effects so as to ascertain the relative importance of T-S wave disturbances in a more industrially relevant flow settings. Having said that, this study has clearly been successful in that we have been able to clearly demonstrate that flows of this nature are indeed susceptible to disturbances in the form of Tollmien-Schlichting waves, confirming the earlier speculation of Bhattacharyya and Gupta[14].

ACKNOWLEDGMENTS

DATA AVAILABILITY STATEMENT

The data that support the findings of this study are available from the corresponding author upon reasonable request.

REFERENCES

[1] B. C. Sakiadis, "Boundary-layer behavior on continuous solid surfaces: II. The boundary layer on a continuous flat surface," AIChE J. **7**, 221 (1961).

[2] S. L. Waters, "Solute uptake through the walls of a pulsating channel," J. Fluid Mech. **433**, 193 (2001).

[3] J. Vleggaar, "Laminar boundary layer behaviour on continuous, accelerating surfaces," Chem. Engng Sci. **32**, 1517 (1977).

[4] L. J. Crane, "Flow past a stretching plate," Zeit. Angew. Math. Phys. **21**, 645 (1970).

[5] C. Y. Wang, "The three-dimensional flow due to a stretching flat surface," Phys. Fluids **27**, 1915 (1984).

[6] R. Ayats, F. Marques, A. Meseguer, and P. D. Weidman, "Flows between orthogonally stretching parallel plates," Phys. Fluids **33**, 024103 (2021).

[7] E. Magyari and B. Keller, "Heat and mass transfer in the boundary layers on an exponentially stretching continuous surface," J. Phys. D: Appl. Phys. **32**, 577 (1999).

[8] P. S. Gupta and A. S. Gupta, "Heat and mass transfer on a stretching sheet with suction or blowing," Can. J. Chem. Engng **55**, 744 (1977).

[9] T. T. Al-Housseiny and H. A. Stone, "On boundary-layer flows induced by the motion of stretching surfaces," J. Fluid Mech. **706**, 597 (2012).

[10] A. Chakrabarti and A. S. Gupta, "Hydromagnetic flow and heat transfer over a stretching sheet," Q. Appl. Math. **37**, 73 (1979).

[11] K. R. Rajagopal, T. Y. Na, and A. S. Gupta, "Flow of a viscoelastic fluid over a stretching sheet," Rheol. Acta **23**, 213 (1984).

[12] N. Riley and P. D. Weidman, "Multiple solutions of the Falkner-Skan equation for flow past a stretching boundary," SIAM J. Appl. Math. **49**, 1350 (1989).

[13] S. Liao, "On the analytic solution of magnetohydrodynamic flows of non-Newtonian fluids over a stretching sheet," J. Fluid Mech. **488**, 189 (2003).

[14] S. N. Bhattacharyya and A. S. Gupta, "On the stability of viscous flow over a stretching sheet," Q. Appl. Math. **18**, 359 (1985).

[15] H. S. Takhar, M. Ali, and A. S. Gupta, "Stability of magnetohydrodynamic flow over a stretching sheet," in *Liquid Metal Magnetohydrodynamics*, Vol. 10, edited by J. J. Lielpeteris and R. J. Moreau (Springer Netherlands, Dordrecht, 1989) Chap. 57, pp. 465–471, 1st ed.

[16] B. S. Dandapat, L. E. Holmedal, and H. I. Andersson, "Stability of flow of a viscoelastic fluid over a stretching sheet," Arch. Mech. **46**, 829 (1994).

[17] J. M. Davis and C. Pozrikidis, "Linear stability of viscous flow induced by surface stretching," Arch. Appl. Mech. **84**, 985 (2014).

[18] R. J. Lingwood, "Absolute instability of the boundary layer on a rotating disk," J. Fluid Mech. **299**, 17 (1995).

[19] P. J. Schmid and D. S. Henningson, *Stability and Transition in Shear Flows* (Springer, 2001).

[20] R. Miller, S. J. Garrett, P. T. Griffiths, and Z. Hussain, "Stability of the Blasius boundary layer over a heated plate in a temperature-dependent viscosity flow," Phys. Rev. Fluids **3**, 113902 (2018).

[21] L. J. Porter, *The Effects of Passive Wall Porosity on the Linear Stability of Boundary Layers*, Ph.D. thesis, University of Warwick (1998).

[22] L. J. Dempsey and A. G. Walton, "Vortex/Tollmien–Schlichting wave interaction states in the asymptotic suction boundary layer," Q. J. Mech. App. Math. **70**, 187 (2017).

[23] F. T. Smith, "Non-parallel flow stability of the Blasius boundary layer," Proc. R. Soc. Lond. A **366**, 91 (1979).

[24] W. H. Reid, "The Stability of Parallel Flows," in *Basic Developments in Fluid Dynamics*, Vol. 1, edited by M. Holt (Academic Press, London, 1965) Chap. 3, pp. 249–307, 1st ed.

[25] J. J. Healey, "On the neutral curve of the flat-plate boundary layer: comparison between experiment, Orr–Sommerfeld theory and asymptotic theory," J. Fluid Mech. **288**, 59 (1995).

[26] M. Cracco, C. Davies, and T. N. Phillips, "Linear stability of the flow of a second order fluid past a wedge," Phys. Fluids **32**, 084102 (2020).